ATLAS NOTE

ATLAS-CONF-2013-007

March 1, 2013
Minor Revision: March 10, 2013

Search for strongly produced supersymmetric particles in final states with two same-sign leptons and jets with the ATLAS detector using 21 fb^{-1} of proton–proton collisions at $\sqrt{s}$ = 8 TeV

The ATLAS Collaboration

Abstract

A search for the production of supersymmetric particles decaying into final states with jets, b-jets, missing transverse momentum and two isolated leptons, e or μ, with the same electric charge (same-sign leptons) is presented. The analysis uses a data sample collected during 2012, which corresponds to a total integrated luminosity of 20.7 fb^{-1} of $\sqrt{s}$ = 8 TeV proton–proton collisions recorded with the ATLAS detector at the Large Hadron Collider. No deviation from the Standard Model expectation is observed. Exclusion limits are derived for a mSUGRA/CMSSM model, which is compatible with a mass of around 126 GeV for the lightest Higgs boson, and for a wide variety of simplified models of supersymmetry. The result significantly extends previous exclusion limits from several searches for Supersymmetry.

A technical problem has been found in the pseudo-experiments used to make Table 4 in the version of March 1. The excluded range in that table is somewhat expanded and the text includes a minor correction. None of the figures or conclusions have been changed.

1 Introduction

Supersymmetry (SUSY) [1–9] predicts new bosonic partners for the fermions and fermionic partners for the bosons of the Standard Model (SM). In the MSSM [10–14], which is an R-parity conserving minimal supersymmetric extension of the SM, the lightest supersymmetric particle (LSP) is stable and weakly interacting, and SUSY particles are pair-produced in proton–proton collisions. In a large variety of models, the LSP is the lightest neutralino, $\tilde{\chi}_1^0$. The coloured superpartners of quarks and gluons, the squarks ($\tilde{q}$) and gluinos ($\tilde{g}$), are expected to be produced in strong interaction processes at the Large Hadron Collider (LHC). Their decays via cascades ending with the LSP would produce striking experimental signatures. The undetected LSP results in missing transverse momentum ($\boldsymbol{p}_{\mathrm{T}}^{\mathrm{miss}}$ and its magnitude $E_{\mathrm{T}}^{\mathrm{miss}}$). The final states also contain multiple jets and possibly leptons. In this note, events with two leptons of the same electric charge (same-sign leptons) and multiple jets are used to search for strongly produced supersymmetric particles. This search is motivated by the fact that gluinos are Majorana fermions, which implies that, when produced in pairs, their decay chains have a high probability to produce same-sign (SS) lepton pairs.

In the MSSM, the scalar partners of right-handed and left-handed quarks, $\tilde{q}_R$ and $\tilde{q}_L$, can mix to form two mass eigenstates, $\tilde{q}_1$ and $\tilde{q}_2$, where $\tilde{q}_1$ denotes the lighter particle. The RL mixing effect is proportional to the corresponding SM fermion masses and therefore becomes important for the third generation. Large mixing can yield a bottom squark, $\tilde{b}_1$, and a top squark, $\tilde{t}_1$, mass eigenstates which are significantly lighter than other squarks. Light $\tilde{t}_1$ and $\tilde{b}_1$ squarks, and gluinos are also favoured by natural SUSY [15, 16]. Consequently, $\tilde{b}_1$ and $\tilde{t}_1$ could be produced with large cross sections at the LHC, either directly in pairs, or through $\tilde{g}\tilde{g}$ production with subsequent $\tilde{g} \to b\tilde{b}_1$ or $\tilde{g} \to t\tilde{t}_1$ decays (gluino-mediated production). Several possible decay chains can lead to same-sign leptons. For instance, the gluino-mediated top squark production, followed by the decay $\tilde{t}_1 \to t\tilde{\chi}_1^0$, leads to four top quarks in the final state, which can produce same-sign lepton pairs when decaying leptonically. Alternatively, the decay via a chargino ($\tilde{\chi}_1^{\pm}$) , $\tilde{t}_1 \to b\tilde{\chi}_1^{\pm} \to bW^{\pm}\tilde{\chi}_1^0$ can also lead to same-sign lepton pairs. Since the production of same-sign lepton pairs is rare in the Standard Model, searches based on this signature benefit from low background.

With the expected final states, the search utilizes same-sign electron and muon pairs (ee, $e\mu$, $\mu\mu$), missing transverse momentum, b-quark jets (b-jets) and multiple high-p_{T} jets. Three event classes are distinguished depending on the number of jets identified as originating from b-quark decays; zero (b-jet veto) , ≥ 1 or ≥ 3 b-jets. Background to these event classes arises from Standard Model processes with pairs of real isolated same-sign leptons, for instance from $t\bar{t} + W/Z$ and from $W^{\pm}W^{\pm}$, WZ and ZZ processes (diboson). Other backgrounds (mainly from $t\bar{t}$) consist of one real lepton and another fake lepton, which denotes hadrons mis-identified as leptons, leptons originating from heavy flavour decays, and electrons from photon conversions. A third class of background arises from a mis-measurement of the lepton charge, mainly from Z/γ^* and $t\bar{t}$ production processes.

The current analysis follows the method used for the earlier ATLAS publication made with 2.05 fb^{-1} at 7 TeV [17], and the one using 5.8 fb^{-1} at 8 TeV [18], but it has a substantially increased sensitivity since it uses the full 2012 data set of 20.7 fb^{-1} at 8 TeV. In addition, identification of the b-jets (b-tagging) is used, and more signal regions are introduced and optimized to consider a wider variety of signal models.

2 SUSY models

The results of the measurement are interpreted in model independent limits on the event yields from new physics processes in the signal regions. Additionally, model dependent exclusion limits are provided in the parameter space of several SUSY models.

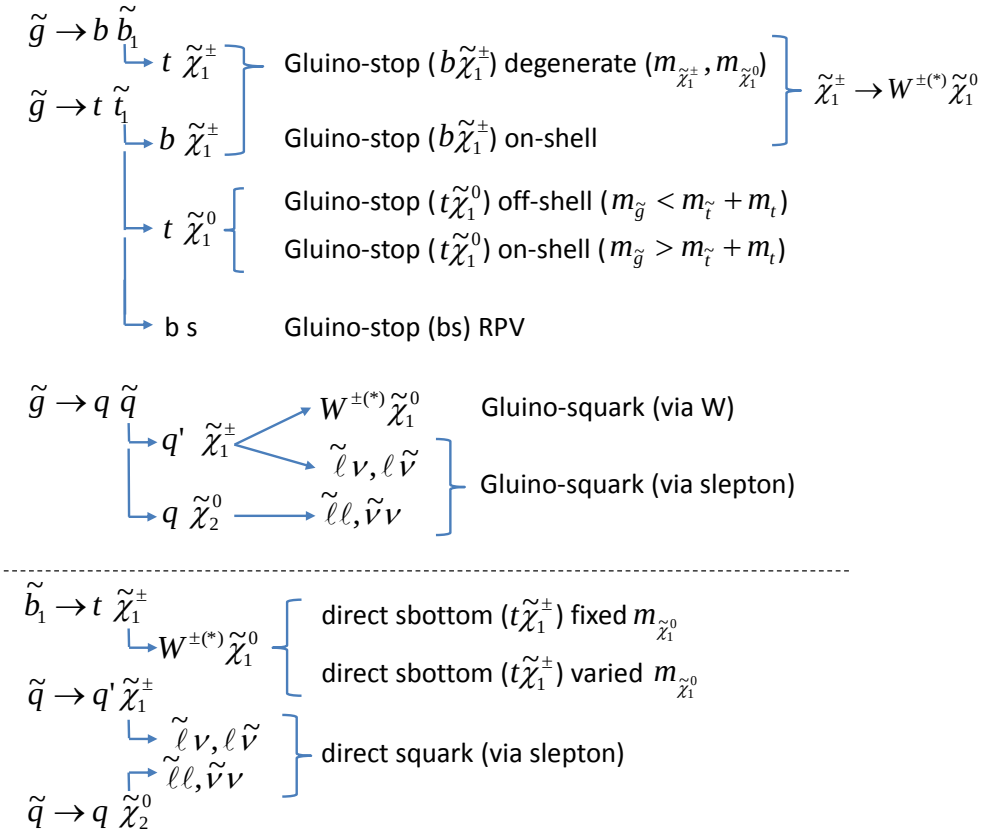

Figure 1: Overview of the simplified models considered in the analysis. The common feature is the strong pair production of supersymmetric particles, e.g. $pp \to \tilde{g}\tilde{g}$, $\tilde{b}\bar{\tilde{b}}$ or $\tilde{q}\bar{\tilde{q}}$. They differ in the decay sequences and mass assignments.

The first model considered is the **mSUGRA/CMSSM** model [19–24] with the parameters $\tan(\beta) = 30$, $A_0 = -2\,m_0$ and $\mu > 0$, which can accommodate a lightest Higgs boson mass around 126 GeV. Only strong production and associated electroweak (gluino-gaugino, squark-gaugino) processes are included. Results are expressed as a function of m_0 and $m_{1/2}$.

Moreover, model dependent limits are derived in several simplified SUSY models. Figure 1 shows a summary of the models considered in this note. They are characterized by strong pair production of the supersymmetric partners of the gluon, b-quark and light quarks. The first class of simplified models are the gluino-stop models, where gluinos are produced in pairs and decay into a $t\tilde{t}_1$ pair (or a $b\tilde{b}_1$ pair, in one of the models considered) with a branching ratio of 100%. The models differ in the decay chain of the $\tilde{t}_1$ and in the sparticle masses. Prompt leptons are produced in top quark decays. In the second class gluinos are also produced in pairs, but they decay into $q\tilde{q}$ with leptons produced either via W bosons or sleptons. The third class considers direct production of bottom squark pairs, leading to prompt leptons from W bosons and top quarks. The fourth class describes the pair production of first or second generation squarks ($\tilde{q}$) yielding prompt leptons from slepton decays.

The simplified models have the following detailed properties:

In the **Gluino-stop ($t\tilde{\chi}_1^0$) off-shell ($m_{\tilde{g}} < m_{\tilde{t}} + m_t$)** model, gluinos are produced in pairs and assumed to be lighter than all squark flavours. The top squark $\tilde{t}_1$ is the lightest squark. Gluinos decay through mediation of a virtual (off-shell) top squark to a pair of top quarks and the lightest neutralino (LSP),

$\tilde{g} \to t\tilde{t}^* \to t\bar{t}\,\tilde{\chi}_1^0$. In the simulation the mass of the top squark is set to $m_{\tilde{t}_1} = 2.5$ TeV and the masses of all other squarks are much higher (decoupled). The final state is therefore characterized by the presence of four top quarks and two LSPs. Same-sign leptons are expected to result from top quark decays. Results are interpreted in the parameter space of the gluino and LSP masses.

The **Gluino-stop ($t\tilde{\chi}_1^0$) on-shell ($m_{\tilde{g}} > m_{\tilde{t}} + m_t$)** model is similar to the previous one, but the top squark $\tilde{t}_1$ is lighter than $m_{\tilde{g}} - m_t$. Thus the gluino decays into an on-shell $\tilde{t}_1$, which decays further into $t\,\tilde{\chi}_1^0$. The neutralino mass is set to 60 GeV. The final state contains four top quarks and two LSPs. Same-sign leptons are expected to result from top quark decays. Limits are expressed as a function of the gluino and $\tilde{t}_1$ masses.

In the **Gluino-stop ($b\tilde{\chi}_1^\pm$) on-shell** model the $\tilde{t}_1$ is the lightest squark, all other squarks are heavier than the gluino and $m_{\tilde{g}} > m_{\tilde{t}_1} + m_t$, such that the decay $\tilde{g} \to \tilde{t}_1 t$ has a branching ratio of 100%. Top squarks are assumed to decay exclusively via $\tilde{t}_1 \to b\tilde{\chi}_1^\pm$. The chargino mass is set to 120 GeV and the neutralino mass to 60 GeV, hence the chargino $\tilde{\chi}_1^\pm$ decays through a virtual W boson ($\tilde{\chi}_1^\pm \to W^{*\pm}\tilde{\chi}_1^0$) into a three-body final state. Therefore the gluino decays via the sequence $\tilde{g} \to t\tilde{t}_1 \to tb\tilde{\chi}_1^\pm \to tbW^{*\pm}\tilde{\chi}_1^0$, leading to final states with pairs of top and bottom quarks, LSPs and decay products of the virtual W bosons. Same-sign leptons are expected to result from top quark decays and the W bosons. Limits are expressed as a function of the gluino and $\tilde{t}_1$ masses.

In the **Gluino-stop ($b\tilde{\chi}_1^\pm$) degenerate ($m_{\tilde{\chi}^\pm}, m_{\tilde{\chi}^0}$)** model, gluinos are assumed to be lighter than all squarks and $\tilde{t}_1$ and $\tilde{b}_1$ are the lightest squarks. Pair production of gluinos is the only process taken into account, with gluinos decaying via virtual stops or sbottoms with a branching ratio of 100% assumed for $\tilde{t}_1^* \to b\tilde{\chi}_1^\pm$ and $\tilde{b}_1^* \to t\tilde{\chi}_1^\mp$, respectively. A small mass difference ($\Delta M = 2$ GeV) is assumed between $\tilde{\chi}_1^\pm$ and $\tilde{\chi}_1^0$, such that $\tilde{\chi}_1^\pm$ decays into $\tilde{\chi}_1^0$ plus very soft particles X. Therefore, both chains of gluino decays $\tilde{g} \to t\tilde{t}^* \to tb\tilde{\chi}_1^\pm \to tb\tilde{\chi}_1^0 + X$ and $\tilde{g} \to b\tilde{b}^* \to bt\tilde{\chi}_1^\mp \to bt\tilde{\chi}_1^0 + X$ effectively result into the same three-body final state ($tb\tilde{\chi}_1^0$) with similar kinematics. The final state is characterized by the presence of two top, two bottom quarks and two LSPs. Same-sign leptons can arise from the decays of the top quarks (which can be of the same charge). The results are interpreted as a function of the gluino and LSP masses.

The **Gluino-stop (bs) RPV** model [25] considers the production of gluino pairs with subsequent gluino decays to $t\tilde{t}$. Top squarks are assumed to decay with an R-parity and baryon number violating $\lambda''_{323} = 1$ coupling as $\tilde{t} \to sb$. Other squarks are not considered in this simplified model. Gluino pair production dominates for all but very light top squarks, and the only decay mode is $\tilde{g} \to t\tilde{t} \to tsb$. The final state consists of two top quarks, two b-jets and two light quark jets and moderate missing transverse momentum. Same-sign lepton combinations can arise from top decays. Limits are expressed as function of the gluino and top squark masses.

The **Gluino-squark (via W)** model describes $\tilde{g}\tilde{g}$ production with a subsquent gluino decay $\tilde{g} \to q\tilde{q}$. The squark decays further into a quark and chargino, which in turn decays into a W boson and the LSP. The chargino mass is related to the LSP mass by $m_{\tilde{\chi}^\pm} = 2 \cdot m_{\tilde{\chi}^0}$. From the gluino decay chain $\tilde{g} \to q\tilde{q} \to qqW\tilde{\chi}_1^0$ one expects final states with four light jets, two W bosons, two LSPs and no b-jets. Prompt same-sign leptons in the event can arise from the decays of the W bosons. Limits are expressed as a function of the gluino and LSP masses.

The **Gluino-squark (via sleptons)** model again considers $\tilde{g}\tilde{g}$ production. The gluino decays with equal probability as $\tilde{g} \to q\tilde{q} \to qq\,\tilde{\chi}_1^\pm$ or $\tilde{g} \to q\tilde{q} \to qq\,\tilde{\chi}_2^0$. Then the $\tilde{\chi}_1^\pm$ decays with equal probability into a slepton and a neutrino or into a lepton and a sneutrino. The $\tilde{\chi}_2^0$ decays with equal probability into a slepton and a lepton or a neutrino and a sneutrino. Finally the slepton decays into a lepton and a $\tilde{\chi}_1^0$, or the sneutrino decays into a neutrino and a $\tilde{\chi}_1^0$. The masses of the $\tilde{\chi}_1^\pm$ and $\tilde{\chi}_2^0$ are assumed to be equal

to the average of the gluino and the LSP masses, and the slepton and sneutrino masses are assumed to be equal to the average of the $\tilde{\chi}_1^{\pm}/\tilde{\chi}_2^0$ and the LSP masses. All three flavours of sleptons are considered and are degenerate in mass. Squark masses are assumed to be much larger than the gluino masses. The decay chains

$$\begin{aligned}
\tilde{g} &\rightarrow qq\,\tilde{\chi}_1^{\pm} \rightarrow qq\tilde{\ell}\nu \rightarrow qq\ell\nu\tilde{\chi}_1^0 \\
\tilde{g} &\rightarrow qq\,\tilde{\chi}_1^{\pm} \rightarrow qq\ell\tilde{\nu} \rightarrow qq\ell\nu\tilde{\chi}_1^0 \\
\tilde{g} &\rightarrow qq\,\tilde{\chi}_2^0 \rightarrow qq\ell\tilde{\ell} \rightarrow qq\ell\ell\tilde{\chi}_1^0 \\
\tilde{g} &\rightarrow qq\,\tilde{\chi}_2^0 \rightarrow qq\nu\tilde{\nu} \rightarrow qq\nu\nu\tilde{\chi}_1^0
\end{aligned}$$

can lead to events with up to two charged leptons in the final state. Thus final states can contain four light jets, up to four charged leptons and missing transverse energy. Prompt same-sign lepton pairs can appear via the slepton or gaugino decays. Limits are expressed in the parameter space of gluino and LSP masses.

The **Direct sbottom ($t\tilde{\chi}_1^{\pm}$)** model assumes that only direct pair production of bottom squarks is relevant and a bottom squark decays only via $\tilde{b} \rightarrow t+\tilde{\chi}_1^{\mp}$ followed by the chargino decay $\tilde{\chi}_1^{\mp} \rightarrow W^{(*)\mp}+\tilde{\chi}_1^0$. The **fixed $m_{\tilde{\chi}^0}$** model assumes $m_{\tilde{\chi}^0} = 60$ GeV and the **varied $m_{\tilde{\chi}^0}$** model $m_{\tilde{\chi}^0} = m_{\tilde{\chi}^{\pm}}/2$. Final states consist of pairs of top quarks, W bosons (real or virtual) and missing transverse momentum. Same-sign dilepton combinations arise from the decays of the top quarks and the W bosons. Limits are expressed as a function of the $\tilde{b}$ and $\tilde{\chi}_1^{\pm}$ masses.

Finally the **Direct-squark (via sleptons)** model is similar to the Gluino-squark (via slepton) model. However, in this case the first step is the direct pair production of $\tilde{q}$ (first and second generation only) followed by the decays $\tilde{q} \rightarrow q\,\tilde{\chi}_1^{\pm}$ or $\tilde{q} \rightarrow q\,\tilde{\chi}_2^0$ with equal probability. The same mass assignments for $\tilde{\chi}_1^{\pm}$, $\tilde{\chi}_2^0$, sleptons and sneutrinos and the same decays for the $\tilde{\chi}_1^{\pm}$ and the $\tilde{\chi}_2^0$ are used as in the Gluino-squark (via slepton) model.

The resulting decay chains are

$$\begin{aligned}
\tilde{q} &\rightarrow q\,\tilde{\chi}_1^{\pm} \rightarrow q\tilde{\ell}\nu \rightarrow q\ell\nu\tilde{\chi}_1^0 \\
\tilde{q} &\rightarrow q\,\tilde{\chi}_1^{\pm} \rightarrow q\ell\tilde{\nu} \rightarrow q\ell\nu\tilde{\chi}_1^0 \\
\tilde{q} &\rightarrow q\,\tilde{\chi}_2^0 \rightarrow q\ell\tilde{\ell} \rightarrow q\ell\ell\tilde{\chi}_1^0 \\
\tilde{q} &\rightarrow q\,\tilde{\chi}_2^0 \rightarrow q\nu\tilde{\nu} \rightarrow q\nu\nu\tilde{\chi}_1^0\,.
\end{aligned}$$

Final states contain two light jets, up to four charged leptons and missing transverse momentum. Prompt same-sign dilepton combinations can appear via the slepton or gaugino decays. Limits are expressed in the parameter space of the squark and LSP masses.

3 Signal and background simulation

Simulated Monte Carlo (MC) events are used to model the SUSY signal efficiency, to optimize the event selection requirements and to aid in the description of the Standard Model backgrounds. Only backgrounds which produce prompt same-sign leptons are estimated from MC simulation, i.e. $t\bar{t}$ production plus bosons ($W/Z/H$) and diboson production plus jets. Samples of $t\bar{t}V$+jets, $t\bar{t}$+WW and VVV+jets ($V = W, Z$) are generated with MadGraph [26] interfaced to Pythia [27]. Pythia8 [28] is used to model $t\bar{t}H$ production. VV+jets production is modeled with Sherpa v1.4.1 [29] and contain matrix elements for up to three final state partons. These samples use the default Sherpa parametrization for the renormalization and factorization scales and require a dilepton invariant mass $m_{\ell\ell} > 0.1$ GeV. The theoretical

cross sections are normalized to NLO calculations and the uncertainties are estimated to be 30% for the $t\bar{t}W$ and $t\bar{t}Z$ (motivated by [30]), and 7% for diboson production (computed with MCFM [31] with scale, PDF and α_s uncertainties taken into account). Other sources of background such as $t\bar{t}$(+jets), W/Z+jets, $W\gamma$, $t\bar{t}\gamma$ and single-top production are estimated with data-driven methods.

The SUSY signal samples were generated with the HERWIG++ [32] and MadGraph programs using the PDF set CTEQ6L1 [33]. Signal cross sections are calculated to next-to-leading order in the strong coupling constant, adding the resummation of soft gluon emission at next-to-leading-logarithmic accuracy (NLO+NLL) [34–38]. The nominal cross section and the uncertainty are taken from an envelope of cross section predictions using different PDF sets and factorization and renormalization scales, as described in Ref. [39]. The theoretical uncertainties of SUSY signal processes depend on the parameter choices; they are typically around 25% for gluino pair production and 15% for squark pair production.

The simulation includes the effect of multiple pp interactions and is weighted to reproduce the observed distribution of the average number of collisions per bunch crossing. MC samples are processed through a detector simulation [40] based on Geant4 [41] or on a fast simulation using a parameterisation of the performance of the ATLAS electromagnetic and hadronic calorimeters [42]. Simulated events are reconstructed in the same manner as the data.

4 Event selection and reconstruction

The ATLAS detector [43] features tracking detectors surrounded by a 2 T superconducting solenoid, calorimeters, and a muon spectrometer in a toroidal magnetic field. The calorimeter system, with acceptance covering the pseudorapidity[1] range $|\eta| < 4.9$, consists of a high-granularity liquid-argon calorimeters with lead, copper, or tungsten absorbers and an iron scintillator calorimeter. Events are selected by a three level trigger system.

4.1 Event selection

Two different trigger strategies are used to cover the full phase space for signal selection and control samples. For the signal regions with the $E_{\mathrm{T}}^{\mathrm{miss}} > 150$ GeV requirement, the $E_{\mathrm{T}}^{\mathrm{miss}}$-only triggers are used, which reach close to 100% efficiency in this region of phase space. For low $E_{\mathrm{T}}^{\mathrm{miss}}$ regions a single lepton trigger is used if the leading lepton has $p_{\mathrm{T}} > 40$ GeV (muons) or $p_{\mathrm{T}} > 70$ GeV (electrons) and a dilepton trigger is employed if the leading lepton p_{T} is below those thresholds. These triggers are chosen to reach plateau efficiencies in the phase space of interest. The electron triggers reach constant efficiencies >95% and muon triggers have constant efficiencies between 75% and 100%, depending on the pseudorapidity region.

Jets are reconstructed from three-dimensional calorimeter energy clusters by using the anti-k_t algorithm [44,45] with a radius parameter of 0.4. Jet energies are corrected [46] for detector inhomogeneities, the non-compensating nature of the calorimeter, and the impact of multiple overlapping pp interactions, using factors derived from test beam, cosmic ray, pp collision data and from the detailed Geant4 detector simulation. Jets are required to have $p_{\mathrm{T}} > 40$ GeV and $|\eta| < 2.8$. If b-tagging is required, the threshold is lowered to $p_{\mathrm{T}} > 20$ GeV and a neural network based b-tagging algorithm [47] with a 70% efficiency operating point is used to identify jets containing a b-hadron decay.

Electron candidates must satisfy the "tight++" selection criteria described in Ref. [48] reoptimized for 2012 data and are required to fulfill $p_{\mathrm{T}} > 20$ GeV, $|\eta| < 2.47$ and to be isolated, i.e. the total p_{T} of additional charged particles or calorimeter energy inside a cone in the $\eta - \phi$ plane of radius

[1]The pseudorapidity is defined in terms of the polar angle θ as $\eta = -\ln\tan(\theta/2)$ and the rapidity is defined as $y = \ln[(E+p_z)/(E-p_z)]/2$. The separation between final state particles is defined as $\Delta R = \sqrt{(\Delta y)^2 + (\Delta\phi)^2}$ and is Lorentz invariant under boosts along the z-axis. The transverse momentum is denoted as p_{T}.

$\Delta R = 0.3$ around the electron must be smaller than 16% and 18%, respectively, of the electron p_{T}. The charged track assigned to the electron candidate must have a longitudinal impact parameter z_0 satisfying $|z_0 \sin\theta| < 0.4$ mm and fulfill the requirement for the significance of the transverse impact parameter of $d_0/\sigma(d_0) < 3$.

Muon candidates are identified by matching an extrapolated inner detector track and one or more track segments in the muon spectrometer [49,50]. They are required to fulfill $p_{\mathrm{T}} > 20$ GeV, $|\eta| < 2.4$ and to be isolated, i.e. similar track and calorimeter isolation requirements are used as for electrons, but with isolation cuts of 12% of the muon momentum. The same impact parameter requirements as for electrons are applied.

To resolve overlaps between reconstructed jets and leptons, jets within a distance of $\Delta R = 0.2$ of an electron candidate are rejected. Furthermore, any lepton candidate with a distance $\Delta R < 0.4$ to the closest remaining jet is discarded.

The calculation of $E_{\mathrm{T}}^{\mathrm{miss}}$ [51] is based on the vectorial sum of the p_{T} of reconstructed objects (jets, leptons, photons) as well as calorimeter energy clusters (with $|\eta| < 4.9$) not belonging to reconstructed objects. A track-based method [52] is applied to suppress event pile-up (additional pp collisions superimposed on the hard physics process from multiple interactions) and to hence improve the $E_{\mathrm{T}}^{\mathrm{miss}}$ resolution.

A primary vertex with a position consistent with the beam spot envelope and made of at least five tracks is required [53]. Events containing cosmic rays and detector noise are rejected using dedicated quality criteria [54]. Events of interest are selected if the two leading leptons passing the requirements described above have the same electric charge.

4.2 Signal region

The signal regions are optimised using the SUSY models listed in Section 2 and employing the following kinematic variables: effective mass, m_{eff}, defined as the scalar sum of the transverse momenta of the two leading leptons, the selected jets and $E_{\mathrm{T}}^{\mathrm{miss}}$; the transverse mass, computed from the leading lepton, ℓ, and the missing transverse momentum as $m_T = \sqrt{2p_{\mathrm{T}}^{\ell}E_{\mathrm{T}}^{\mathrm{miss}}(1-\cos[\Delta\phi(\ell, E_{\mathrm{T}}^{\mathrm{miss}})])}$. Slightly different cuts are applied for model independent limits (discovery case) and model dependent exclusion limits (exclusion case). To derive exclusion limits, the signal regions are made exclusive to each other and are statistically combined.

Three signal regions are defined (see also Table 1 for a detailed specification of the selection requirements):

- **SR0b**: A b-jet veto is applied. Events are required to have at least three jets, and large $E_{\mathrm{T}}^{\mathrm{miss}}$ and transverse mass. Furthermore, a cut on m_{eff} is applied only for the discovery case, whereas for exclusion limits this cut is omitted and a binned shape fit in the m_{eff} distribution is performed.

- **SR1b**: Events are required to contain at least one b-jet and three other jets. The same cuts on $E_{\mathrm{T}}^{\mathrm{miss}}$and m_{T} as for SR0b are applied, but m_{eff} is required to be > 700 GeV.

- **SR3b**: Events are required to contain at least three b-jets and at least four jets for the discovery case. For the exclusion case, at least 5 jets are required and the cuts on $E_{\mathrm{T}}^{\mathrm{miss}}$ and m_{T} of SR0b and SR1b are inverted, in order to make this signal region statistically independent from the other two.

The requirement on the number of jets and b-jets is independent throughout the analysis, i.e. a b-jet may be counted as well in the jet category. SR1b is motivated by the majority of the signatures targeted by this analysis, which correspond to final states with several b-jets. The signal region SR0b with a veto on the presence of b-jets in the event is complementary to SR1b and is sensitive to the gluino-squark and

Signal region	N_{b-jets}	Signal cuts (discovery case)	Signal cuts (exclusion case)
SR0b	0	$N_{jets} \geq 3$, E_T^{miss}> 150 GeV	$N_{jets} \geq 3$, E_T^{miss}> 150 GeV, m_T> 100 GeV,
		m_T> 100 GeV, m_{eff}>400 GeV	binned shape fit in m_{eff} for m_{eff} >300 GeV
SR1b	≥1	$N_{jets} \geq 3$, E_T^{miss}> 150 GeV	$N_{jets} \geq 3$, E_T^{miss}> 150 GeV, m_T>100 GeV,
		m_T>100 GeV, m_{eff}>700 GeV	binned shape fit in m_{eff} for m_{eff}>300 GeV
SR3b	≥3	$N_{jets} \geq 4$	$N_{jets} \geq 5$,
		-	E_T^{miss}< 150 GeV or m_T< 100 GeV

Table 1: Definition of the signal regions. The cuts for the discovery and exclusion cases are shown separately. For all signal regions, two leading leptons with $p_T > 20$ GeV and of the same electric charge are required. Jets are selected with $p_T > 40$ GeV while b-jets are required to have $p_T > 20$ GeV.

direct squark models, which do not result in enhanced production of b-quarks. The b-jet veto helps to suppress the $t\bar{t}$-like background, which otherwise dominates the event selection with several jets. The third signal region, SR3b, does not require large values of E_T^{miss}, m_{eff} or m_T. It is therefore targeted at compressed regions of the phase-space (i.e. small mass differences) in models involving third generation squarks, which feature large b-jet multiplicities and small missing transverse momentum.

5 Backgrounds

5.1 Background estimation

Searches in events with two same-sign leptons are characterized by very low backgrounds. Three main classes of backgrounds can be distinguished: prompt same-sign lepton pairs, charge mis-measurement and fake leptons.

SM sources of events of prompt same-sign leptons with jets arise mainly from the production of a W or Z boson, decaying leptonically, in association with $t\bar{t}$, where at least one of the top quarks decays leptonically, and from diboson background (WZ, ZZ) in association with jets. These backgrounds are estimated from MC.

Background from charge mis-measurement consists of events with two opposite-sign leptons (OS) for which the charge of an electron is mis-identified. The dominant mechanism of charge mis-identification is due to the radiation of a hard photon bremsstrahlung followed by an asymmetric conversion for which the electron with the opposite charge dominates ($e^{\pm} \rightarrow e^{\pm}\gamma \rightarrow e^{\pm}e^{\pm}e^{\mp}$). The probability of mis-identifying the charge of a muon is negligible. Previous studies [17, 18] show that the background from lepton charge mis-measurement is dominated by dilepton $t\bar{t}$ events. It is estimated in this analysis using a fully data-driven technique to determine the charge flip probability as function of the electron p_T and η from Drell-Yan events. The rate is measured using the ratio of SS to OS electron pairs with an invariant mass compatible with the Z boson within 15 GeV. The probability of electron charge mis-measurement is found to vary from approximately 10^{-4} to 0.02 in the range $0 \leq |\eta| \leq 2.5$ and $20 < p_T < 200$ GeV. For the background estimation, this probability is then applied to data regions with the same kinematic requirements as the signal regions but with opposite-sign leptons.

Previous studies [18] show that the fake lepton background is dominated by $t\bar{t}$ events where one lepton comes from the decay of a b-hadron and the other from one of the W bosons. This background

is estimated from the data using a similar method as in Ref. [17] by loosening the lepton identification and isolation criteria, yielding classes of "tight" and "loose" leptons. The method counts the number of observed events containing loose-loose, loose-tight, tight-loose and tight-tight lepton pairs (pairs are ordered by p_{T}). Using four linear equations, the number of events in the signal region with combinations of fake and prompt lepton pairs can be determined. The parameters of the equations contain two types of probabilities for electrons and muons separately: the probability for a loose fake lepton and the probability for a loose prompt lepton to pass the tight selection criteria. These probabilities are measured as a function of the lepton p_{T} and η from data. The prompt lepton probabilities are determined from a data sample enriched with prompt leptons from $Z \to \ell^+\ell^-$ decays, obtained by requiring $80\,\mathrm{GeV} < m_{\ell\ell} < 100\,\mathrm{GeV}$. The fake lepton probabilities are measured from a data set enriched with one prompt muon (by requiring $p_{\mathrm{T}} > 40\,\mathrm{GeV}$) and an additional fake lepton. The electron fake rate is determined from two samples of SS $e\mu$ events, one with a b-jet veto and another with at least one tagged b-jet. The muon must pass tight selection cuts, whereas the electron must have $20\,\mathrm{GeV} < p_{\mathrm{T}} < 40\,\mathrm{GeV}$. The muon fake rate is determined from a sample of SS dimuon events with $20\,\mathrm{GeV} < p_{\mathrm{T}} < 40\,\mathrm{GeV}$, where at least one of the two muons is required to pass the tight selection criteria. The systematic uncertainty of the fake lepton background includes the extrapolation of the fake rate to higher lepton p_{T} and the dependency of the fake rate on the event selection.

The signal region SR3b, which requires ≥ 3 b-jets and ≥ 4 jets, is dominated by events containing at least one mistagged b-jet. Studies of simulated $t\bar{t}$ events indicate that the fake lepton rate increases with increasing b-tag multiplicity. Since there is not enough statistics in the data to measure the fake lepton rate in regions with ≥ 3 b-tags, the fake lepton rate, as obtained from events with at least one b-tag, is multiplied by a factor $1.5^{+1.5}_{-0.75}$ and extrapolated to the signal region SR3b. This factor is determined from $t\bar{t}$ Monte Carlo studies with MC@NLO [55] interfaced to HERWIG [56], using JIMMY [57] for the underlying event. The large systematic uncertainty is motivated by the uncertainty of Monte Carlo estimates for fake leptons and by the limited statistics.

Several systematic uncertainties on the background estimates have been evaluated. For the charge mis-measurement background, the main uncertainties come from the statistical uncertainty of the charge flip probability measurements and from a potential systematic bias of the data driven method which is estimated with Monte Carlo simulations. For fake leptons, the main uncertainties come from the statistical uncertainty of the loose-to-tight probability measurements, the subtraction of background from charge mis-measurement and prompt leptons, and from a potential systematic bias estimated by varying the event selection of the loose-to-tight measurements with Monte Carlo simulations. Finally, for prompt same-sign lepton pairs, the main uncertainties come from systematic variations of the jet energy scale, b-tagging efficiency, trigger efficiency, lepton identification efficiency and pile-up modelling in the Monte Carlo simulations. Additional uncertainties are assigned corresponding to different acceptance predictions from alternative generators. For $t\bar{t}$+V production MadGraph is compared with Alpgen. For diboson production Sherpa is compared with PowHeg. The process $W^{\pm}W^{\pm}$ is not included in the PowHeg diboson simulation, but simulated separately with MadGraph interfaced to Pythia. For the 2012 data set the preliminary uncertainty of the integrated luminosity is ±3.6% based on the calibration procedure described in Ref. [58].

5.2 Validation of background estimates

The background estimates obtained from Monte Carlo simulations and data driven techniques are checked in events with two same-sign leptons, where the leptons are selected as described in Section 4.1. Figure 2–4 show the control plots for the ee, $e\mu$ and $\mu\mu$ channels respectively . Figure 2 shows the jet and b-jet multiplicity distributions for the ee channel with individual contributions of the major background classes. Good agreement is found between data and the SM expectation. The uncertainty bands include statistical and systematic uncertainties. Similarly, Figure 3 shows as validation plots for the $e\mu$-channel

the missing transverse momentum distribution for events with at least one b-jet and the lepton p_{T} distribution for events with a b-jet veto. Finally, for the di-muon channel Figure 4 displays the effective mass distribution with a veto on b-jets and the transverse mass distribution for events with at least one b-jet. For all channels good agreement between data and background prediction is obtained within the estimated systematic uncertainties. In addition, to validate the Monte Carlo description of events with high b-jet multiplicity containing both real and fake b-tags, a sample of events containing opposite-sign dilepton pairs and ≥ 3 b-jets has been studied. Distributions have been found to agree well, in particular the p_{T} distributions of the b-jets.

Three regions are devised to validate the dominant backgrounds of the prompt same-sign leptons, which are estimated by Monte Carlo simulation, i.e. $t\bar{t}W$, $t\bar{t}Z$ and dibosons. These validation regions are not used to constrain these backgrounds in the fits to the signal regions but to verify the validity of the MC predictions.

The validation region for $t\bar{t}W$ (VR-ttW) uses exactly two same-sign muons (no electrons) to reduce the background of fake leptons and charge mis-measurement. The event selection requires one or more jets with $p_{\mathrm{T}} > 30$ GeV, exactly two b-jets with $p_{\mathrm{T}} > 20$ GeV, $20 < E_{\mathrm{T}}^{\mathrm{miss}} < 120$ GeV and a transverse mass $m_{\mathrm{T}} > 80$ GeV.

The validation region for $t\bar{t}Z$ (VR-ttZ) requires three leptons (e or μ), where the two leading leptons must have $p_{\mathrm{T}} > 20$ GeV and the third lepton $p_{\mathrm{T}} > 10$ GeV. A pair of opposite-sign, same-flavour leptons is required with the invariant mass of 83 GeV $< m_{\ell^+\ell^-} <$ 96 GeV. In addition, the event selection requires two or more jets with $p_{\mathrm{T}} > 40$ GeV, one or two b-jets with $p_{\mathrm{T}} > 20$ GeV, $20 < E_{\mathrm{T}}^{\mathrm{miss}} < 120$ GeV and $m_{\mathrm{eff}} > 300$ GeV.

The dibosons validation region (VR-diboson) requires two same-sign muons to reduce the fake and charge mis-measurement backgrounds. In addition, the event selection requires two or more jets with $p_{\mathrm{T}} > 20$ GeV, no tagged b-jet with $p_{\mathrm{T}} > 20$ GeV, $20 < E_{\mathrm{T}}^{\mathrm{miss}} < 120$ GeV and a transverse mass of $m_{\mathrm{T}} > 100$ GeV.

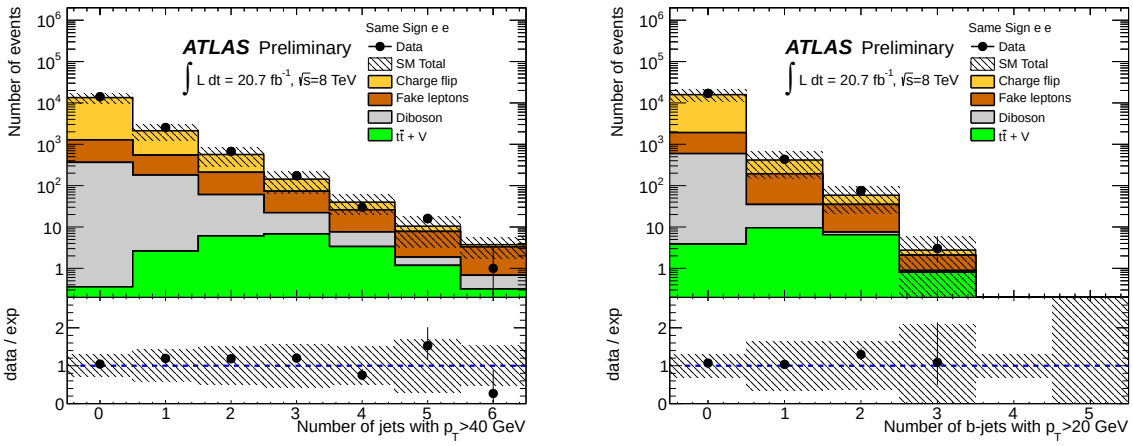

Figure 2: *ee* channel: Distributions of the jet multiplicity ($p_{\mathrm{T}} > 40$ GeV) (left) and of the b-jet multiplicity ($p_{\mathrm{T}} > 20$ GeV) (right).

The number of observed events and expected events from background sources are shown in Table 2 for each validation region. The uncertainties on the number of expected background events include systematic uncertainties (cf. Section 5.1). Figure 5 shows the effective mass distributions in the diboson and in the combined VR-ttW and VR-ttZ validation regions. The background checks in the validation region provide confidence that the MC simulations predict the SM background rate of prompt like-sign lepton pairs in events with multiple jets and b-jets within a factor of approximately 2, where the accuracy

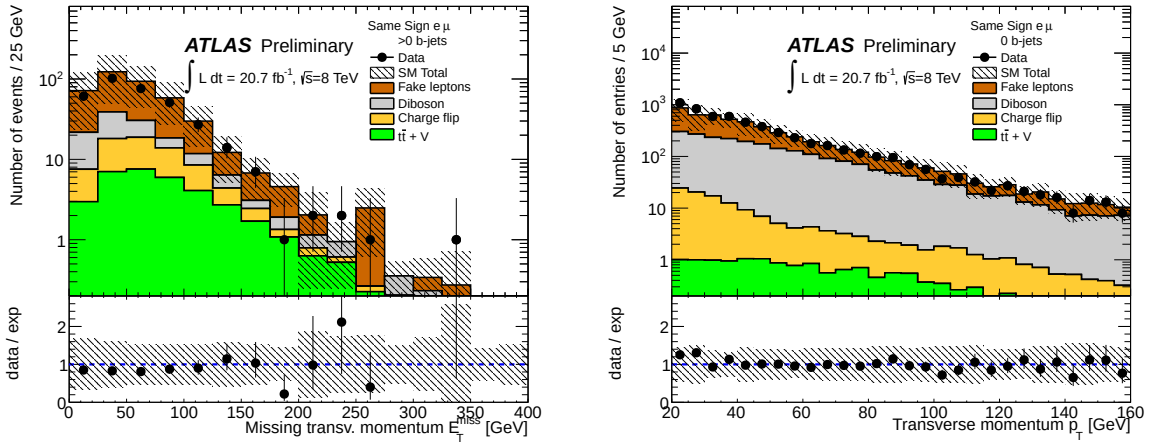

Figure 3: $e\mu$ channel: Missing transverse momentum distribution after lepton selection with at least one b-jet (left). Distributions of the p_{T} of the selected leptons with a b-jet veto (right).

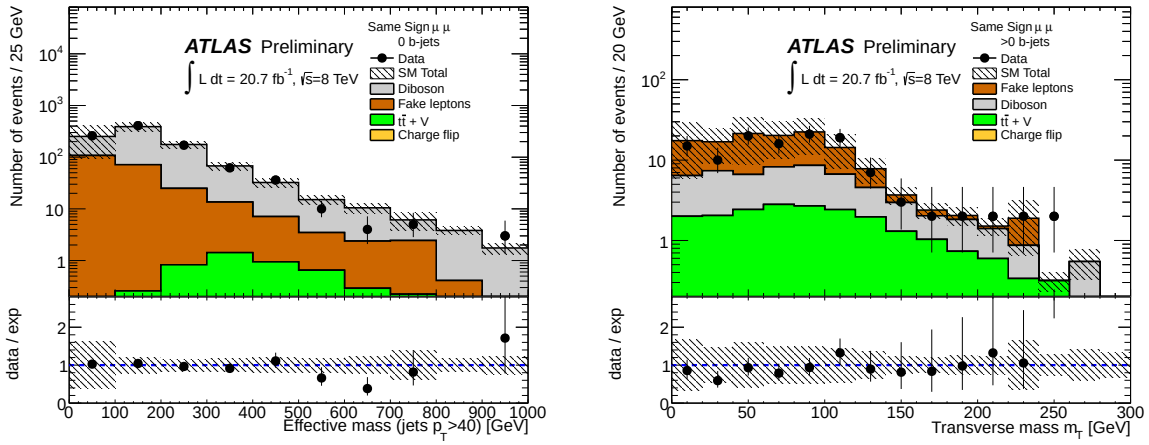

Figure 4: $\mu\mu$ channel: Effective mass distribution after lepton selection with a veto on b-jets (left). Transverse mass distribution after lepton selections with at least one b-jet (right).

is limited by the data statistics in the validation region. Monte Carlo simulations show that in general the expected contamination from SUSY signal processes in the validation regions is small, but for specific models like the Direct sbottom model it can be as large as $\sim 25\%$ in the VR-ttW region.

6 Results

Table 3 presents the number of observed events and expected background events in the three signal regions for the discovery (upper table) and exclusion cases (lower table). The background for the SR0b region is dominated by events containing fake leptons and dibosons (both with large uncertainties). In signal regions SR1b and SR3b the largest background contribution and uncertainty is expected from $t\bar{t}+V$ events. The p_0 values indicate the p-value of the measurement for the background only hypothesis. Good agreement is observed between the data and the SM expectation. A comparison of tables A and B shows, that the event sample for the exclusion case has a larger background contribution from fake leptons in SR1b. This is due to the relaxed m_{eff} cut in the exclusion case sample. Figure 6 shows the effective mass

Event classes	VR-diboson	VR-ttW	VR-ttZ
Observed events	54	9	4
Expected background events	74 ± 13	4.2 ± 1.9	8.0 ± 2.0
Expected $t\bar{t}$+V events	1.6 ± 0.8	2.7 ± 1.5	3.2 ± 1.1
Expected diboson events	60 ± 7	0.4 ± 0.1	3.9 ± 1.3
Expected fake lepton events	12 ± 11	1.1 ± 1.1	0.9 ± 0.5
Expected charge mis-meas. events	0	0	0

Table 2: Number of observed data events and expected events from background sources in the validation regions (VR-diboson, VR-ttW and VR-ttZ). The quoted background errors include statistical and systematic uncertainties.

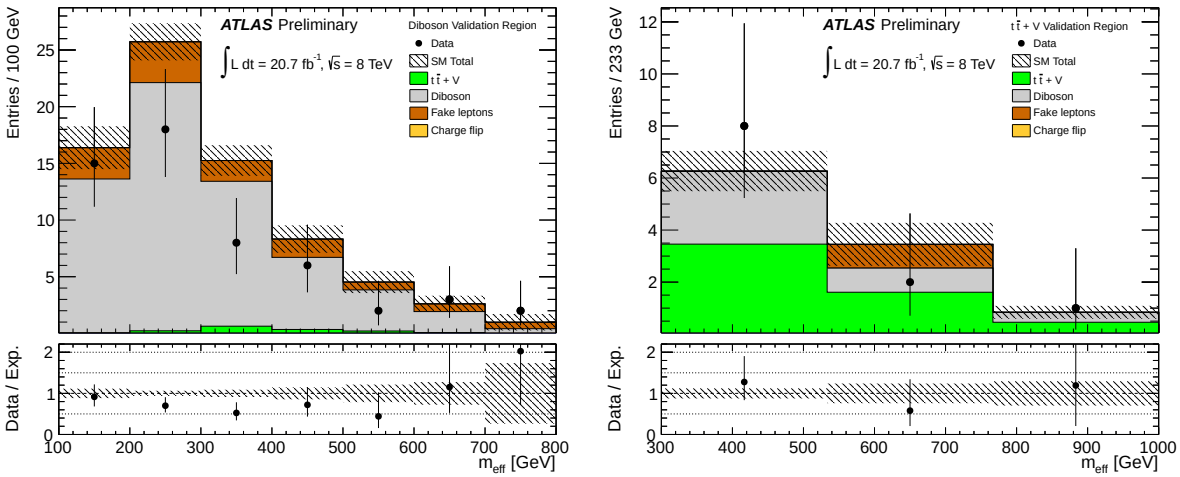

Figure 5: Effective mass distributions in the VR-dibosons (left) and sum of VR-ttW and VR-ttZ (right).

distribution for SR0b and SR1b using the exclusion case cuts. The fake lepton background contributes mainly at low m_{eff} in SR1b.

7 Interpretations

Since the observed number of events in the signal regions agrees with the SM expectation, the data are used to place model independent upper limits on the number of signal events and on the visible cross-section ($\epsilon\sigma$), where ϵ denotes the product of acceptance and efficiency. In addition, model dependent exclusion limits are provided in a mSUGRA/CMSSM model and in simplified models as described in Section 2. All limits are determined with a fit based on the profile likelihood method using asymptotic formulae [59] and correspond to 95% CL limits using the CL_s [60] calculation. For the model independent limits, the main results are calculated using pseudo-experiments and the asymptotic formulae are used for comparisons.

7.1 Model-independent limits

The model-independent upper limits based on the observed and expected number of events in the signal regions for the discovery case, and calculated with pseudo-experiments, are shown in Table 4. $\langle\epsilon\sigma\rangle^{95}_{\text{obs}}$ is

A) Discovery case	**SR0b**	**SR1b**	**SR3b**
Observed events	5	8	4
Expected background events	7.5 ± 3.3	3.7 ± 1.6	3.1 ± 1.6
Expected $t\bar{t}$ + V events	0.5 ± 0.4	2.2 ± 1.0	1.7 ± 0.8
Expected diboson events	3.4 ± 1.0	0.7 ± 0.4	0.1 ± 0.1
Expected fake lepton events	3.4 ± 3.1	$0.3^{+1.1}_{-0.3}$	$0.9^{+1.4}_{-0.9}$
Expected charge mis-measurement events	0.1 ± 0.1	0.5 ± 0.2	0.4 ± 0.1
p_0	0.50	0.11	0.36

B) Exclusion case	**SR0b**	**SR1b**	**SR3b**
Observed events	5	11	1
Expected background events	7.5 ± 3.2	10.1 ± 3.9	1.8 ± 1.3
Expected $t\bar{t}$ + V events	0.5 ± 0.4	3.4 ± 1.5	0.6 ± 0.4
Expected diboson events	3.4 ± 1.1	1.4 ± 0.7	< 0.1
Expected fake lepton events	3.4 ± 2.9	4.4 ± 3.1	1.0 ± 1.1
Expected charge mis-measurement events	0.2 ± 0.1	0.8 ± 0.3	0.1 ± 0.1
p_0	0.5	0.39	0.5

Table 3: Number of observed data events and expected backgrounds for the signal regions SR0b, SR1b and SR3b. The event counts correspond to the signal selection for the discovery limits (table A) and the exclusion limits (table B). p_0 denotes the p-value of the observed events for the background only hypothesis. The quoted background errors include statistical and systematic uncertainties.

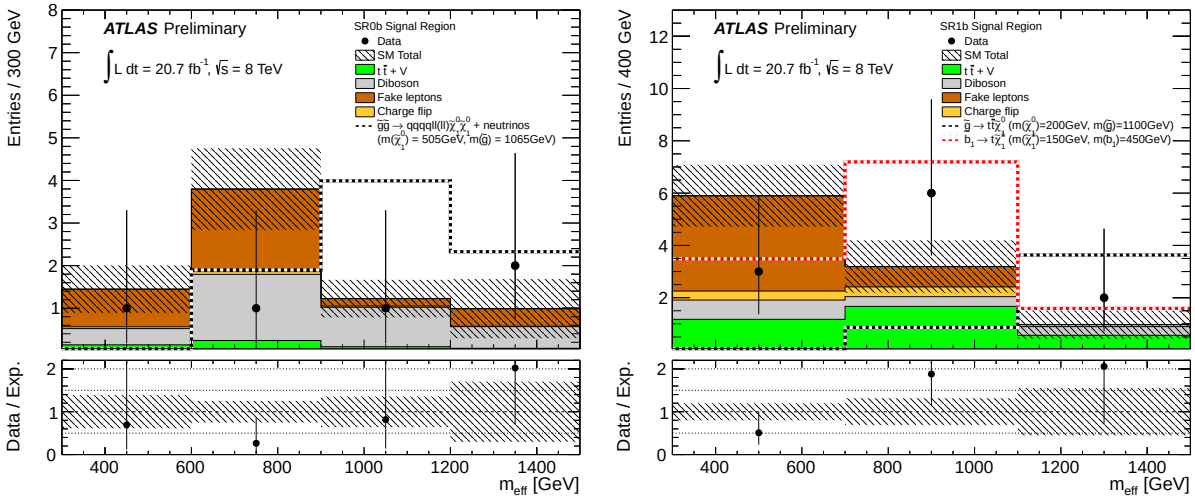

Figure 6: Effective mass distributions in the signal regions SR0b (left) and SR1b (right) using the exclusion case event sample. The last bin includes overflows.

the 95% CL upper limit on the visible cross section. $S^{95}_{\rm obs}$ and $S^{95}_{\rm exp}$ are the observed and expected 95% CL upper limits on the number of signal events. With asymptotic formulae, the corresponding observed (expected) 95% CL upper limits on the number of signal events in SR0b, SR1b and SR3b are 6.5 (7.7), 10.8 (6.5) and 6.7 (5.9), respectively.

Signal regions	$\langle\epsilon\sigma\rangle^{\mathbf{95}}_{\mathbf{obs}}$ **[fb]**	$\mathbf{S^{95}_{obs}}$	$\mathbf{S^{95}_{exp}}$
SR0b	0.33	6.7	$7.9^{+2.6}_{-2.0}$
SR1b	0.53	11.0	$6.8^{+2.6}_{-1.5}$
SR3b	0.34	7.0	$5.9^{+2.4}_{-1.3}$

Table 4: Upper 95% CL limits on the visible cross-section ($\langle\epsilon\sigma\rangle^{95}_{\rm obs}$) and on the observed ($S^{95}_{\rm obs}$) and expected ($S^{95}_{\rm exp}$) number of signal events. The event sample for the discovery case is used for this calculation, as defined in Section 4.2

7.2 Model-dependent limits

The measurement is used to place model-dependent exclusion limits in the context of several SUSY models. For these limits, the exclusion case event sample is used, as described in Section 4.2. A simultaneous fit to all three signal regions using the binned $m_{\rm eff}$ distribution, shown in Figure 6 for the signal regions SR0b and SR1b, is used to calculate the exclusion limits for each model.

mSUGRA/CMSSM

Figure 7 presents the 95% CL exclusion limits for the mSUGRA/ CMSSM model in the (m_0, $m_{1/2}$) parameter space. The yellow band around the expected limit shows the $\pm1\sigma$ uncertainty region including all statistical and systematic uncertainties except the theoretical uncertainties on the SUSY cross section. The $\pm1\sigma^{\rm SUSY}_{\rm theory}$ lines around the observed limit are obtained by changing the SUSY cross section by $\pm1\sigma$. All mass limits of supersymmetric particles quoted later in this section are derived from the $-1\sigma^{\rm SUSY}_{\rm theory}$ line. Figure 7 shows that the measurement allows to exclude a large region of the mSUGRA/CMSSM parameter space.

Gluino-stop ($t\tilde{\chi}^{\mathbf{0}}_{\mathbf{1}}$) off-shell

Results for the Gluino-stop ($t\tilde{\chi}^0_1$) off-shell model are presented in the $m_{\tilde{g}}$-$m_{\tilde{\chi}^0}$ plane. Figure 8 (left) displays the observed and expected limits for each individual signal region and the combined limits. The grey numbers show the limits on the excluded model cross sections. The exclusion lines show the interplay between SR1b, which performs best at a large mass difference between the gluino and the LSP, and SR3b, which performs best at a small mass difference (compressed region) between the gluino and the LSP. Gluinos are excluded with 95% CL up to masses of 900 – 1020 GeV for LSP masses below 550 GeV. The right figure shows the improved limits compared to previous results obtained with a similar analysis but with 5.8 fb^{-1} at $\sqrt{s}$ = 8 TeV, for which the exclusion limit for the gluino mass reached 800–890 GeV and 360 GeV for the neutralino mass (see [18]). For comparison, results for this model from other ATLAS searches using $\sqrt{s}$=8 TeV data are also shown. These were based on events with ≥ 3 b-jets and no leptons [61] or 3 leptons and more than 4 jets [62]. This analysis improves the excluded region for gluino masses between 800 and 1000 GeV and near the diagonal in the gluino-neutralino mass plane.

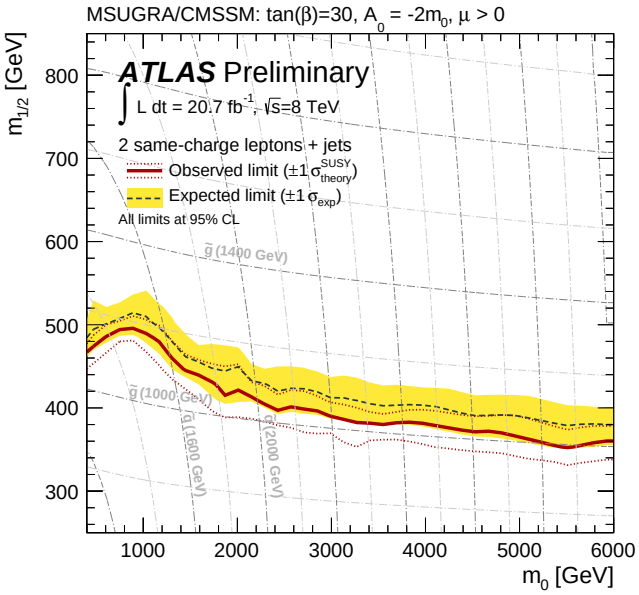

Figure 7: Expected and observed exclusion limits in the mSUGRA/CMSSM model with $\tan(\beta) = 30$, $A_0 = -2m_0$, $\mu > 0$ obtained with 20.7 fb^{-1} at $\sqrt{s}$=8 TeV. All limits are computed at 95% CL.

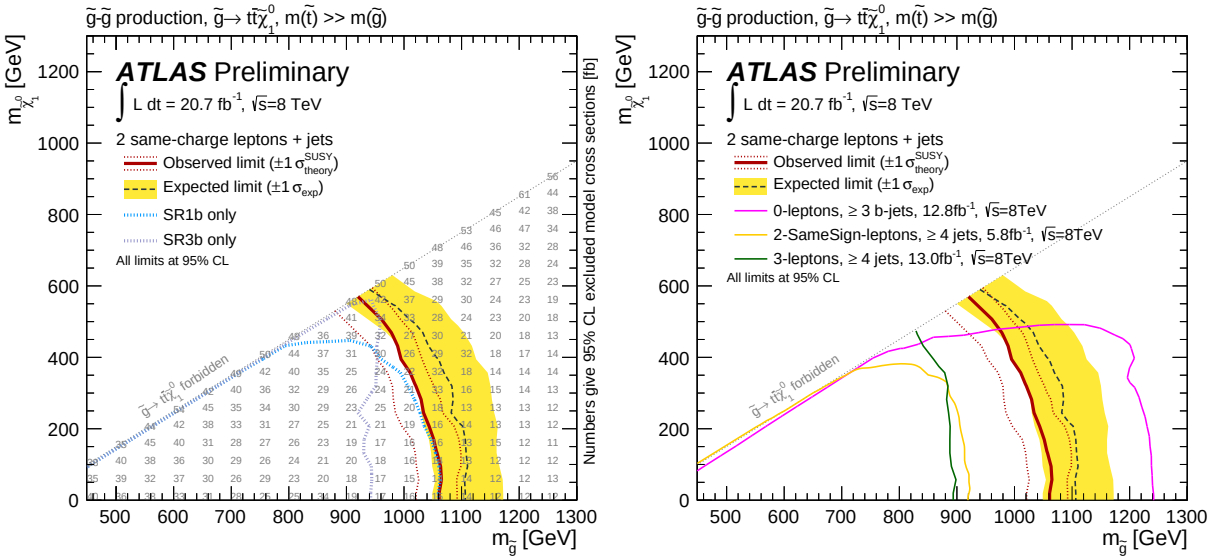

Figure 8: Expected and observed limits for the Gluino-stop ($t\tilde{\chi}_1^0$) off-shell model obtained with 20.7 fb^{-1} at $\sqrt{s}$=8 TeV. The left figure shows the individual exclusion limits for each signal region. The numbers give the limits on the excluded model cross sections. The right figure compares these results with the limits obtained by the most sensitive ATLAS searches with 2012 data [61, 62]. All limits are computed at 95% CL.

Gluino-stop ($t\tilde{\chi}_1^0$) on-shell

Results for the Gluino-stop ($t\tilde{\chi}_1^0$) on-shell model are presented in the $m_{\tilde{t}}$-$m_{\tilde{g}}$ plane. Observed and expected exclusion limits are shown in Figure 9. The model assumes that the top squark decays to top and LSP with $m_{\tilde{\chi}^0} = 60$ GeV. Gluinos are excluded with 95% CL in this model up to masses of about 1030 GeV

for stop masses below 750 GeV.

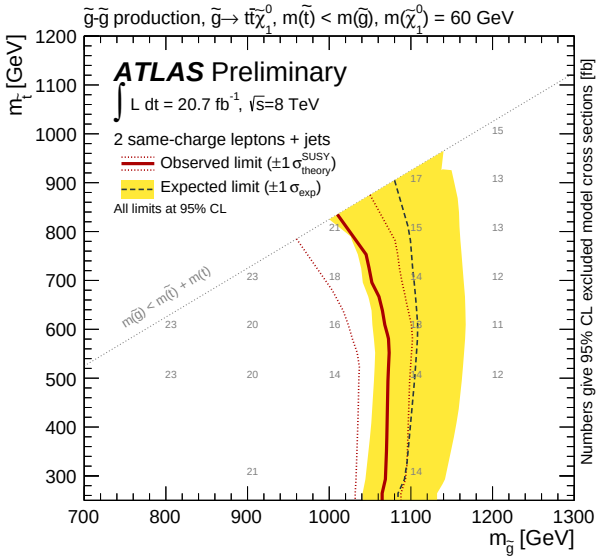

Figure 9: Expected and observed limits for the Gluino-stop ($t\tilde{\chi}_1^0$) on-shell model obtained with 20.7 fb^{-1} at $\sqrt{s}$=8 TeV. The numbers give the limits on the excluded model cross sections. All limits are computed at 95% CL.

Gluino-stop ($b\tilde{\chi}_1^{\pm}$) on-shell

Figure 10 presents the exclusion limits for the Gluino-stop ($b\tilde{\chi}_1^{\pm}$) on-shell model in the $m_{\tilde{t}}$-$m_{\tilde{g}}$ plane. Gluinos are excluded up to masses of about 940 – 1000 GeV for stop masses below 750 GeV. Gluino masses below 850 GeV have been excluded already by a previous ATLAS analysis in the three b-jet channel [63].

Gluino-stop ($b\tilde{\chi}_1^{\pm}$) degenerate ($m_{\tilde{\chi}^{\pm}}, m_{\tilde{\chi}^0}$)

Figure 11 shows the 95% CL observed and expected exclusion limits in the $m_{\tilde{g}}$-$m_{\tilde{\chi}_1^0}$ plane for the Gluino-stop ($b\tilde{\chi}_1^{\pm}$) degenerate model. Gluino masses below 750 – 830 GeV are excluded for LSP masses up to 450 GeV. This measurement improves the previous ATLAS result [61] mainly in the region near the diagonal line of the $m_{\tilde{g}}$-$m_{\tilde{\chi}_1^0}$ plane.

Gluino-stop (bs) RPV

Results for the Gluino-stop (bs) RPV model are presented in the $m_{\tilde{t}}$-$m_{\tilde{g}}$ plane in Figure 12. Expected events in this model are characterized by small missing traverse momentum and several b-jets. Signal region SR3b offers therefore the best sensitivity. Gluino masses are excluded below about 860 GeV over the whole range of considered top squark masses (up to 1 TeV).

Gluino-squark (via W)

The observed and expected 95% CL exclusion limits for the Gluino-squark (via W) model are shown in Figure 13 in the $m_{\tilde{\chi}_1^0}$-$m_{\tilde{g}}$ plane. Gluino masses are excluded below 750–800 GeV for LSP masses up to 450 GeV. This measurement improves an earlier ATLAS result [64] mainly for high LSP masses.

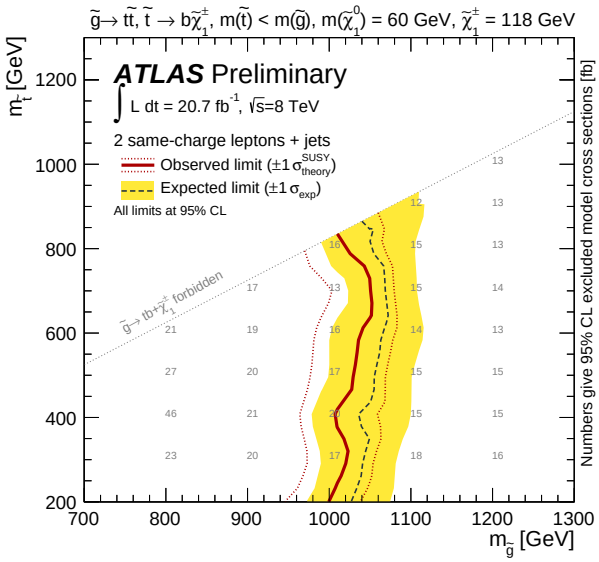

Figure 10: Expected and observed limits for the Gluino-stop ($b\tilde{\chi}_1^{\pm}$) on-shell model obtained with 20.7 fb^{-1} at $\sqrt{s}$=8 TeV. The numbers give the limits on the excluded model cross sections. All limits are computed at 95% CL.

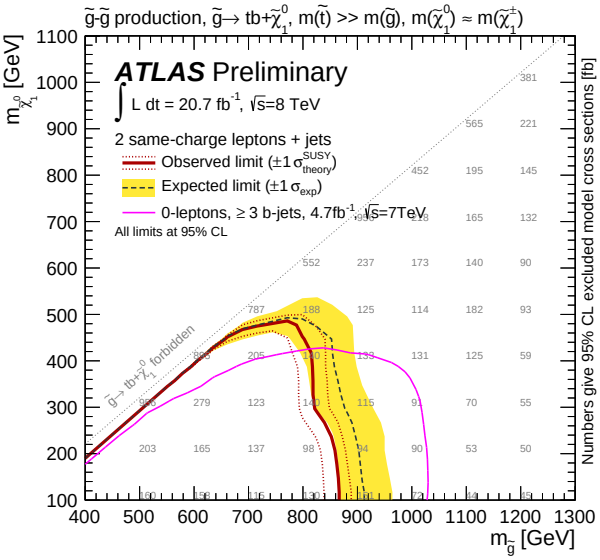

Figure 11: Expected and observed limits for the "Gluino-stop ($b\tilde{\chi}_1^{\pm}$) degenerate" model obtained with 20.7 fb^{-1} at $\sqrt{s}$=8 TeV. The figure shows a comparison with the limits set in [61]. The numbers give the limits on the excluded model cross sections. All limits are computed at 95% CL.

Gluino-squark (via slepton)

Results for the Gluino-squark (via slepton) model are presented in the $m_{\tilde{g}}$- $m_{\tilde{\chi}_1^0}$ plane in Figure 14. Gluino masses up to 1000–1100 GeV are excluded with 95% CL for LSP masses up to 650 GeV. This search significantly improves the existing ATLAS limits for this model [64].

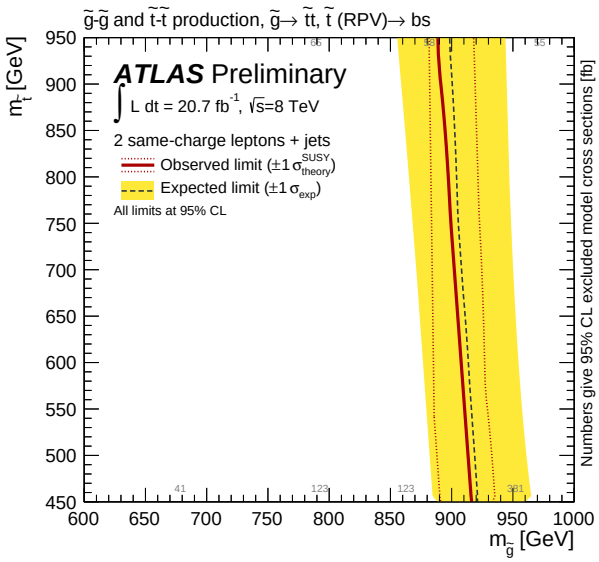

Figure 12: Expected and observed limits for the Gluino-stop (bs) RPV model obtained with 20.7 fb^{-1} at $\sqrt{s}$=8 TeV. The numbers give the limits on the excluded model cross sections. All limits are computed at 95% CL.

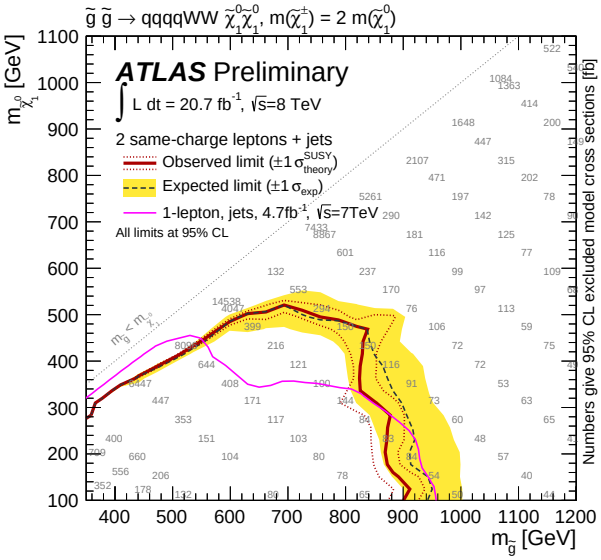

Figure 13: Expected and observed limits for the Gluino-squark (via W) model obtained with 20.7 fb^{-1} at $\sqrt{s}$=8 TeV. The figure shows a comparison with previous ATLAS exclusion limits published in [64]. The numbers give the limits on the excluded model cross sections. All limits are computed at 95% CL.

Direct sbottom ($t\tilde{\chi}_1^{\pm}$)

Results for the Direct sbottom ($t\tilde{\chi}_1^{\pm}$) model are presented in Figure 15 in the $m_{\tilde{b}}$-$m_{\tilde{\chi}_1^{\pm}}$ plane for two different assumptions on the neutralino mass: $m_{\tilde{\chi}_1^0}$ = 60 GeV ("fixed $m_{\tilde{\chi}^0}$" model) and $m_{\tilde{\chi}_1^0} = m_{\tilde{\chi}_1^{\pm}}/2$ ("varied $m_{\tilde{\chi}^0}$" model). Under the assumption $m_{\tilde{\chi}_1^0}$ = 60 GeV, bottom squark masses of 470-480 GeV are excluded with 95% CL for chargino masses below 280 GeV. Similar limits on bottom squark masses are obtained in the "varied $m_{\tilde{\chi}^0}$" model for chargino masses up to 250 GeV. This search improves the

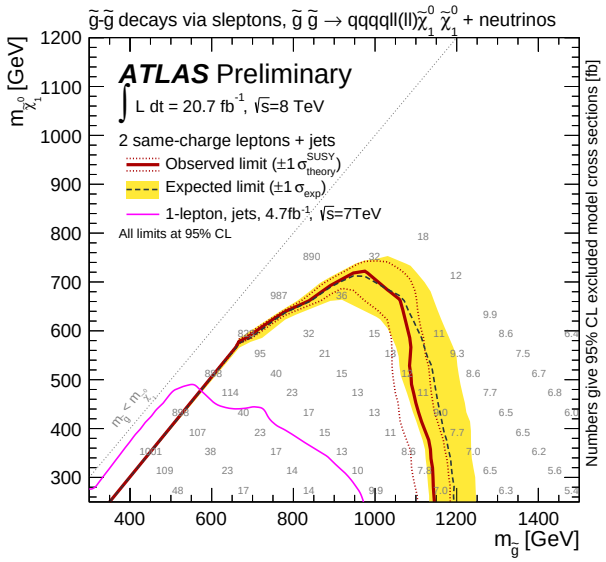

Figure 14: Expected and observed limits for the Gluino-squark (via slepton) model obtained with 20.7 fb^{-1} at $\sqrt{s}$=8 TeV, compared with previous ATLAS results [64]. Note that the previous results were making slightly different assumptions about the relative probabilities of $\tilde{g} \to q\tilde{q} \to qq\,\tilde{\chi}_1^{\pm}$ and $\tilde{g} \to q\tilde{q} \to qq\,\tilde{\chi}_2^0$ decays. The numbers give the limits on the excluded model cross sections. All limits are computed at 95% CL.

existing ATLAS limits for this model [62], computed using 13 fb^{-1}of $\sqrt{s}$=8 TeV data.

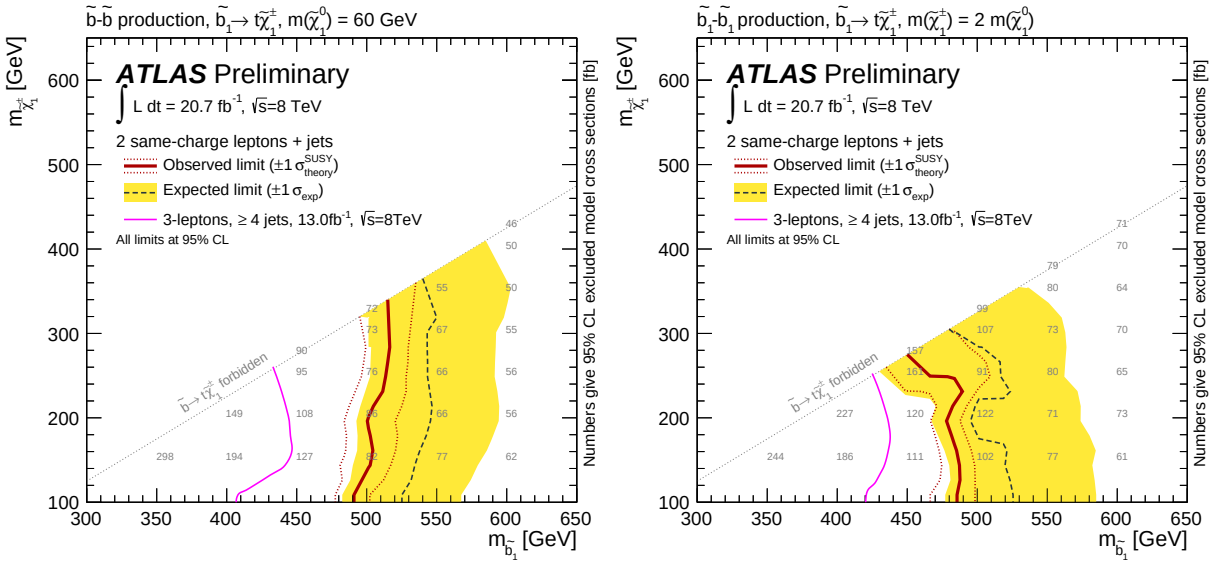

Figure 15: Expected and observed limits for the Direct sbottom ($t\tilde{\chi}_1^{\pm}$) model assuming $m_{\tilde{\chi}_1^0} = 60$ GeV (left) and $m_{\tilde{\chi}_1^0} = m_{\tilde{\chi}_1^{\pm}}/2$ (right) obtained with 20.7 fb^{-1} at $\sqrt{s}$=8 TeV. The plots show a comparison with the limits obtained by the most sensitive ATLAS search [62] with 2012 data. The numbers give the limits on the excluded model cross sections. All limits are computed at 95% CL.

Direct-squark (via slepton)

Observed and expected 95% CL exclusion limits for the Direct-squark (via slepton) model are presented in Figure 16 in the $m_{\tilde{q}}$- $m_{\tilde{\chi}_1^0}$ plane. Squarks masses up to 600-660 GeV are excluded with 95% CL for neutralino masses below 380 GeV.

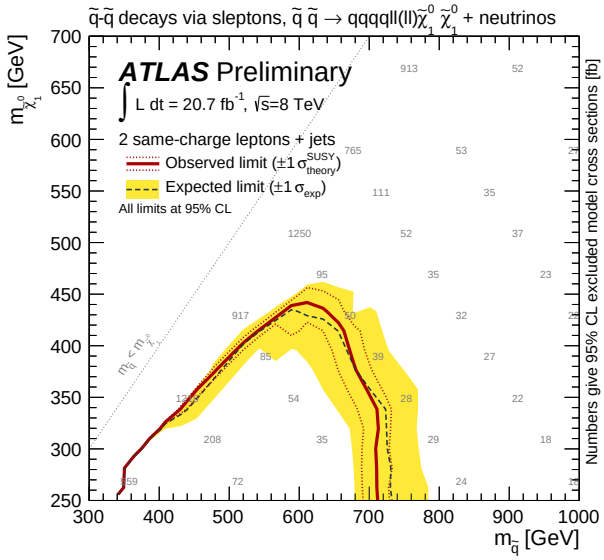

Figure 16: Expected and observed limits for the "Direct-squark (via slepton)" model obtained with 20.7 fb^{-1} at $\sqrt{s}$=8 TeV. The numbers give the limits on the excluded model cross sections. All limits are computed at 95% CL.

8 Conclusions

A search for the production of supersymmetric particles decaying into final states with jets, b-jets, missing transverse momentum and two isolated leptons, e or μ, of the same sign is presented. The analysis uses a data sample collected during 2012 corresponding to a total integrated luminosity of 20.7 fb^{-1} of $\sqrt{s}$ = 8 TeV proton-proton collisions recorded with the ATLAS detector at the Large Hadron Collider. Three signal regions are defined with 0, ≥1 and ≥3 b-jets, respectively. No deviation from the Standard Model expectation is observed. Therefore the results are presented as model-independent limits and as exclusion limits in a mSUGRA/CMSSM model and in several simplified models of supersymmetry. The mSUGRA/CMSSM model is compatible with a mass of the lightest Higgs boson around 126 GeV. The diversity of the simplified models demonstrates the versatility of the analysis. The results put new or significantly improved limits in SUSY parameter regions where the lightest squark can be of the 1^{st}, 2^{nd} or 3^{rd} generations, where the mass differences between the supersymmetric particles can be large or compressed, and where R-parity can be conserved or violated. Hence this analysis covers several important aspects of the searches for supersymmetry at the LHC.

A Cut-flow tables for benchmark signal models

Additional details are provided for three benchmark signal models with 4, 2, and 0 b-jets: Gluino-stop ($t\tilde{\chi}_1^0$) off-shell, Direct sbottom ($t\tilde{\chi}_1^\pm$) and Gluino-squark (via slepton), in order to facilitate future re-interpretations of the results.

A.1 Gluino-stop ($t\tilde{\chi}_1^0$) off-shell

Selection	Electron-Electron Events	Electron-Muon Events	Muon-Muon Events
No cuts	210.3	210.3	210.3
Cleaning	207.4	207.4	207.4
2 leptons	5.3	10.5	5.1
Trigger	5.1	9.8	4.9
$m_{ll} > 12\,\text{GeV}$	5.1	9.8	4.9
Same-sign	1.7	3.3	1.7
$N_{jets40} \geq 3$	1.7	3.2	1.7
SR0b			
$N_{\text{b-jets20}} = 0$	0.1	0.2	0.1
$E_{\text{T}}^{\text{miss}} > 150\,\text{GeV}$	0.1	0.1	0.0
$m_{\text{T}} > 100\,\text{GeV}$	0.1	0.1	0.0
$m_{\text{eff}} > 400\,\text{GeV}$	0.1	0.1	0.0
SR1b			
$N_{\text{b-jets20}} \geq 1$	1.6	3.1	1.6
$E_{\text{T}}^{\text{miss}} > 150\,\text{GeV}$	1.3	2.6	1.4
$m_{\text{T}} > 100\,\text{GeV}$	1.2	2.3	1.2
$m_{\text{eff}} > 700\,\text{GeV}$	1.1	2.2	1.1
SR3b			
$N_{\text{b-jets20}} \geq 3$	0.5	1.3	0.7
$N_{\text{jets40}} \geq 4$	0.5	1.3	0.7

Table 5: Cut-flow for all lepton channels derived from a benchmark point of the model Gluino-stop ($t\tilde{\chi}_1^0$) off-shell, with $m_{\tilde{g}} = 1100$ GeV and $m_{\tilde{\chi}^0}$ =200 GeV. In total 100000 events were generated for this point. The number of events is normalized to the cross-section and to an integrated luminosity of 20.7 fb^{-1}. It also includes weights which are applied to each simulated event separately. In the signal regions the requirements for discovery are used as shown in Table 1.

A.2 Direct-sbottom ($t\chi_1^{\pm}$)

Selection	Electron-Electron Events	Electron-Muon Events	Muon-Muon Events
No cuts	3512.1	3512.1	3512.1
Cleaning	3440.6	3440.6	3440.6
2 leptons	173.7	390.0	217.1
Trigger	163.1	338.5	197.9
$m_{ll} > 12\,\text{GeV}$	162.9	338.0	197.9
Same-sign	50.9	101.9	64.9
$N_{jets40} \geq 3$	44.3	88.9	55.4
SR0b			
$N_{\text{b-jets20}} = 0$	9.4	13.7	7.3
$E_{\text{T}}^{\text{miss}} > 150\,\text{GeV}$	2.8	3.4	2.0
$m_{\text{T}} > 100\,\text{GeV}$	2.2	2.8	1.3
$m_{\text{eff}} > 400\,\text{GeV}$	2.2	2.8	1.3
SR1b			
$N_{\text{b-jets20}} \geq 1$	34.9	75.2	48.1
$E_{\text{T}}^{\text{miss}} > 150\,\text{GeV}$	8.8	23.2	10.6
$m_{\text{T}} > 100\,\text{GeV}$	6.6	16.7	6.2
$m_{\text{eff}} > 700\,\text{GeV}$	5.0	12.4	3.9
SR3b			
$N_{\text{b-jets20}} \geq 3$	3.6	5.5	3.5
$N_{\text{jets40}} \geq 4$	3.5	5.0	2.8

Table 6: Cut-flow for all lepton channels derived from a benchmark point of the Direct-sbottom ($t\tilde{\chi}_1^{\pm}$) model with $m_{\tilde{\chi}_1^0} = 60$ GeV, $m_{\tilde{b}} = 450$ GeV and $m_{\chi_1^{\pm}} = 150$ GeV. In total 20000 events were generated for this point. The number of events is normalized to the cross-section and to an integrated luminosity of 20.7 fb^{-1}. It also includes weights which are applied to each simulated event separately. In the signal regions the requirements for discovery are used as shown in table 1. Note that for this sample a filter is applied at generator level, requiring at least two leptons (e, μ) with $p_{\text{T}} > 10$ GeV and $|\eta| < 2.8$. The efficiency of this filter is about 40.3%.

A.3 Gluino-squark (via slepton)

Selection	Electron-Electron Events	Electron-Muon Events	Muon-Muon Events
No cuts	284.3	284.3	284.3
Cleaning	281.0	281.0	281.0
2 leptons	25.4	20.2	26.2
Trigger	24.3	18.1	24.3
$m_{ll} > 12\,\text{GeV}$	24.3	18.1	24.2
Same-sign	4.6	8.8	4.7
$N_{jets40} \geq 3$	4.3	7.9	4.4
SR0b			
$N_{\text{b-jets20}} = 0$	3.3	5.8	3.1
$E_{\text{T}}^{\text{miss}} > 150\,\text{GeV}$	2.3	4.2	2.1
$m_{\text{T}} > 100\,\text{GeV}$	2.0	3.8	1.9
$m_{\text{eff}} > 400\,\text{GeV}$	2.0	3.8	1.9
SR1b			
$N_{\text{b-jets20}} \geq 1$	1.0	2.1	1.3
$E_{\text{T}}^{\text{miss}} > 150\,\text{GeV}$	0.7	1.5	0.9
$m_{\text{T}} > 100\,\text{GeV}$	0.7	1.4	0.8
$m_{\text{eff}} > 700\,\text{GeV}$	0.7	1.4	0.8
SR3b			
$N_{\text{b-jets20}} \geq 3$	0.0	0.0	0.0
$N_{\text{jets40}} \geq 4$	0.0	0.0	0.0

Table 7: Cut-flow for all lepton channels for model Gluino-squark (via slepton) with $m_{\tilde{g}} = 1065$ GeV, $m_{\tilde{\chi}_1^\pm} = m_{\tilde{\chi}_2^0} = 785$ GeV, $m_{\tilde{\ell}} = 645$ GeV and $m_{\tilde{\chi}_1^0} = 505$ GeV. In total 40000 events were generated for this model point. The number of events is normalized to the cross-section and to an integrated luminosity of 20.7 fb^{-1}. It also includes weights which are applied to each simulated event separately. In the signal regions the requirements for discovery are used as shown in Table 1.

References

[1] H. Miyazawa, *Baryon Number Changing Currents*, Prog. Theor. Phys. **36 (6)** (1966) 1266–1276.

[2] P. Ramond, *Dual Theory for Free Fermions*, Phys. Rev. **D3** (1971) 2415–2418.

[3] Y. A. Golfand and E. P. Likhtman, *Extension of the Algebra of Poincare Group Generators and Violation of p Invariance*, JETP Lett. **13** (1971) 323–326. [Pisma Zh.Eksp.Teor.Fiz.13:452-455,1971].

[4] A. Neveu and J. H. Schwarz, *Factorizable dual model of pions*, Nucl. Phys. **B31** (1971) 86–112.

[5] A. Neveu and J. H. Schwarz, *Quark Model of Dual Pions*, Phys. Rev. **D4** (1971) 1109–1111.

[6] J. Gervais and B. Sakita, *Field theory interpretation of supergauges in dual models*, Nucl. Phys. **B34** (1971) 632–639.

[7] D. V. Volkov and V. P. Akulov, *Is the Neutrino a Goldstone Particle?*, Phys. Lett. **B46** (1973) 109–110.

[8] J. Wess and B. Zumino, *A Lagrangian Model Invariant Under Supergauge Transformations*, Phys. Lett. **B49** (1974) 52.

[9] J. Wess and B. Zumino, *Supergauge Transformations in Four-Dimensions*, Nucl. Phys. **B70** (1974) 39–50.

[10] P. Fayet, *Supersymmetry and Weak, Electromagnetic and Strong Interactions*, Phys. Lett. **B64** (1976) 159.

[11] P. Fayet, *Spontaneously Broken Supersymmetric Theories of Weak, Electromagnetic and Strong Interactions*, Phys. Lett. **B69** (1977) 489.

[12] G. R. Farrar and P. Fayet, *Phenomenology of the Production, Decay, and Detection of New Hadronic States Associated with Supersymmetry*, Phys. Lett. **B76** (1978) 575–579.

[13] P. Fayet, *Relations Between the Masses of the Superpartners of Leptons and Quarks, the Goldstino Couplings and the Neutral Currents*, Phys. Lett. **B84** (1979) 416.

[14] S. Dimopoulos and H. Georgi, *Softly Broken Supersymmetry and SU(5)*, Nucl. Phys. **B193** (1981) 150.

[15] R. Barbieri and G. Giudice, *Upper Bounds on Supersymmetric Particle Masses*, Nucl. Phys. **B306** (1988) 63.

[16] B. de Carlos and J. Casas, *One loop analysis of the electroweak breaking in supersymmetric models and the fine tuning problem*, Phys. Lett. **B309** (1993) 320–328, `arXiv:hep-ph/9303291 [hep-ph]`.

[17] ATLAS Collaboration, *Search for gluinos in events with two same-sign leptons, jets and missing transverse momentum with the ATLAS detector in pp collisions at* $\sqrt{s} = 7$ *TeV*, Phys. Rev. Lett. **108** (2012) 241802, `arXiv:1203.5763 [hep-ex]`.

[18] ATLAS Collaboration, *Search for Supersymmetry in final states with two same-sign leptons, jets and missing transverse momentum with the ATLAS detector in pp collisions at* $\sqrt{s} = 8$ *TeV*, ATLAS-CONF-2012-105. `https://cdsweb.cern.ch/record/1472674`.

[19] A. H. Chamseddine, R. L. Arnowitt, and P. Nath, *Locally Supersymmetric Grand Unification*, Phys. Rev. Lett. **49** (1982) 970.

[20] R. Barbieri, S. Ferrara, and C. A. Savoy, *Gauge Models with Spontaneously Broken Local Supersymmetry*, Phys. Lett. **B119** (1982) 343.

[21] L. E. Ibanez, *Locally Supersymmetric SU(5) Grand Unification*, Phys. Lett. **B118** (1982) 73.

[22] L. J. Hall, J. D. Lykken, and S. Weinberg, *Supergravity as the Messenger of Supersymmetry Breaking*, Phys. Rev. **D27** (1983) 2359–2378.

[23] N. Ohta, *Grand Unified Theories Based on Local Supersymmetry*, Prog. Theor. Phys. **70** (1983) 542.

[24] G. L. Kane, C. F. Kolda, L. Roszkowski, and J. D. Wells, *Study of constrained minimal supersymmetry*, Phys. Rev. **D49** (1994) 6173–6210, arXiv:hep-ph/9312272 [hep-ph].

[25] B. Allanach and B. Gripaios, *Hide and Seek With Natural Supersymmetry at the LHC*, arXiv:1202.6616 [hep-ph].

[26] J. Alwall et al., *MadGraph/MadEvent v4: The New Web Generation*, JHEP **09** (2007) 028, arXiv:0706.2334 [hep-ph].

[27] T. Sjöstrand, S. Mrenna, and P. Z. Skands, *PYTHIA 6.4 Physics and Manual*, JHEP **0605** (2006) 026, arXiv:hep-ph/0603175.

[28] T. Sjostrand, S. Mrenna, and P. Z. Skands, *A Brief Introduction to PYTHIA 8.1*, Comput.Phys.Commun. **178** (2008) 852–867, arXiv:0710.3820 [hep-ph].

[29] T. Gleisberg et al., *Event generation with SHERPA 1.1*, JHEP **02** (2009) 007.

[30] J. M. Campbell and R. K. Ellis, *$t\bar{t}W^{\pm}$ production and decay at NLO*, arXiv:1204.5678 [hep-ph].

[31] J. M. Campbell, R. K. Ellis, and C. Williams, *Vector boson pair production at the LHC*, JHEP **1107** (2011) 018, arXiv:1105.0020 [hep-ph].

[32] M. Bahr et al., *Herwig++ Physics and Manual*, Eur.Phys.J. **C58** (2008) 639–707, arXiv:0803.0883 [hep-ph].

[33] J. Pumplin et al., *New generation of parton distributions with uncertainties from global QCD analysis*, JHEP **07** (2002) 012, arXiv:hep-ph/0201195.

[34] W. Beenakker, R. Hopker, M. Spira, and P. Zerwas, *Squark and gluino production at hadron colliders*, Nucl. Phys. **B492** (1997) 51–103, arXiv:hep-ph/9610490 [hep-ph].

[35] A. Kulesza and L. Motyka, *Threshold resummation for squark-antisquark and gluino-pair production at the LHC*, Phys. Rev. Lett. **102** (2009) 111802, arXiv:0807.2405 [hep-ph].

[36] A. Kulesza and L. Motyka, *Soft gluon resummation for the production of gluino-gluino and squark-antisquark pairs at the LHC*, Phys. Rev. **D80** (2009) 095004, arXiv:0905.4749 [hep-ph].

[37] W. Beenakker et al., *Soft-gluon resummation for squark and gluino hadroproduction*, JHEP **0912** (2009) 041, arXiv:0909.4418 [hep-ph].

[38] W. Beenakker et al., *Squark and gluino hadroproduction*, Int. J. Mod. Phys. **A26** (2011) 2637–2664, arXiv:1105.1110 [hep-ph].

[39] M. Krämer et al., *Supersymmetry production cross sections in pp collisions at* $\sqrt{s} = 7$ *TeV*, arXiv:1206.2892 [hep-ph].

[40] ATLAS Collaboration, *The ATLAS Simulation Infrastructure*, Eur. Phys. J. **C70** (2010) 823–874, arXiv:1005.4568 [physics.ins-det].

[41] S. Agostinelli et al., *GEANT4: A simulation toolkit*, Nucl. Instrum. Meth. **A506** (2003) 250–303.

[42] ATLAS Collaboration, *The simulation principle and performance of the ATLAS fast calorimeter simulation FastCaloSim*, ATL-PHYS-PUB-2010-013. https://cds.cern.ch/record/1300517.

[43] ATLAS Collaboration, *The ATLAS Experiment at the CERN Large Hadron Collider*, JINST **3** (2008) S08003.

[44] M. Cacciari, G. P. Salam, and G. Soyez, *The anti-k_t jet clustering algorithm*, JHEP **04** (2008) 063, arXiv:0802.1189 [hep-ph].

[45] M. Cacciari and G. P. Salam, *Dispelling the N^3 myth for the k_t jet-finder*, Phys. Lett. **B641** (2006) 57–61, arXiv:hep-ph/0512210.

[46] ATLAS Collaboration, *Jet energy measurement with the ATLAS detector in proton-proton collisions at* $\sqrt{s} = 7$ *TeV*, submitted to Eur. Phys. J. C , arXiv:1112.6426 [hep-ex].

[47] ATLAS Collaboration, *Measurement of the b-tag Efficiency in a Sample of Jets Containing Muons with 5 fb^{-1} of Data from the ATLAS Detector*, ATLAS-CONF-2012-043 (2012). https://cdsweb.cern.ch/record/1435197.

[48] ATLAS Collaboration, *Electron performance measurements with the ATLAS detector using the 2010 LHC proton–proton collision data*, Eur. Phys. J. **C72** (2012) 1909, arXiv:1110.3174 [hep-ex].

[49] ATLAS Collaboration, *Muon reconstruction efficiency in reprocessed 2010 LHC proton-proton collision data recorded with the ATLAS detector*, ATLAS-CONF-2011-063. https://cdsweb.cern.ch/record/1345743.

[50] ATLAS Collaboration, *A measurement of the ATLAS muon reconstruction and trigger efficiency using J/psi decays*, ATLAS-CONF-2011-021. https://cdsweb.cern.ch/record/1336750.

[51] ATLAS Collaboration, *Performance of Missing Transverse Momentum Reconstruction in Proton-Proton Collisions at 7 TeV with ATLAS*, Eur. Phys. J. **C72** (2012) 1844, arXiv:1108.5602 [hep-ex].

[52] ATLAS Collaboration, *Performance of missing transverse momentum reconstruction in ATLAS with 2011 proton-proton collisions at* $\sqrt{s} = 7$ *TeV*, ATLAS-CONF-2012-101 (2012). https://cdsweb.cern.ch/record/1463915.

[53] ATLAS Collaboration, *Performance of primary vertex reconstruction in proton-proton collisions at* $\sqrt{s} = 7$ *TeVin the ATLAS experiment*, ATLAS-CONF-2010-069 (2010). hhttp://cdsweb.cern.ch/record/1281344.

[54] ATLAS Collaboration, *Selection of jets produced in proton-proton collisions with the ATLAS detector using 2011 data*, ATLAS-CONF-2012-020 (2012). hhttp://cdsweb.cern.ch/record/1430034.

[55] Frixione, S. and Webber, B. R., *Matching NLO QCD computations and parton shower simulations*, JHEP **06** (2002) 029, arXiv:hep-ph/0204244.

[56] G. Corcella et al., *HERWIG 6: An Event generator for hadron emission reactions with interfering gluons (including supersymmetric processes)*, JHEP **0101** (2001) 010, arXiv:hep-ph/0011363 [hep-ph].

[57] J. Butterworth, J. R. Forshaw, and M. Seymour, *Multiparton interactions in photoproduction at HERA*, Z.Phys. **C72** (1996) 637–646, arXiv:hep-ph/9601371 [hep-ph].

[58] ATLAS Collaboration, *Improved luminosity determination in pp collisions at sqrt(s) = 7 TeV using the ATLAS detector at the LHC*, submitted to Eur. Phys. J. C , arXiv:1302.4393 [hep-ex].

[59] G. Cowan, K. Cranmer, E. Gross, and O. Vitells, *Asymptotic formulae for likelihood-based tests of new physics*, Eur. Phys. J. **C71** (2011) 1554, arXiv:1007.1727 [hep-ph].

[60] A. L. Read, *Presentation of search results: The CL(s) technique*, J. Phys. G **28** (2002) 2693–2704.

[61] ATLAS Collaboration, *Search for gluino pair production in final states with missing transverse momentum and at least three b-jets using 12.8 fb^{-1} of pp collisions at $\sqrt{s}$ = 8 TeV using the ATLAS Detector*, ATLAS-CONF-2012-145. https://cdsweb.cern.ch/record/1493484.

[62] ATLAS Collaboration, *Search for supersymmetry using events with three leptons, multiple jets, and missing transverse momentum in 13.0 fb^{-1} of pp collisions with the ATLAS detector at $\sqrt{s}$ = 8 TeV*, ATLAS-CONF-2012-151. https://cdsweb.cern.ch/record/1493490.

[63] ATLAS Collaboration, *Search for top and bottom squarks from gluino pair production in final states with missing transverse energy and at least three b-jets with the ATLAS detector*, Eur. Phys. J. **C72** (2012) 2174, arXiv:1207.4686 [hep-ex].

[64] ATLAS Collaboration, *Further search for supersymmetry at $\sqrt{s}$ = 7 TeV in final states with jets, missing transverse momentum and isolated leptons with the ATLAS detector*, Phys.Rev. **D86** (2012) 092002, arXiv:1208.4688 [hep-ex].